Title

Proton Traffic Jam: Effect of Nanoconfinement and Acid Concentration on Proton Hopping Mechanism

Journal

ANGEWANDTE CHEMIE-INTERNATIONAL EDITION, 60(48)

ISSN

1433-7851

Authors

Adams, Ellen M
Hao, Hongxia
Leven, Itai
et al.

Publication Date

2021

DOI

10.1002/anie.202108766

Peer reviewed

How to cite: *Angew. Chem. Int. Ed.* **2021**, *60*, 25419–25427
International Edition: doi.org/10.1002/anie.202108766
German Edition: doi.org/10.1002/ange.202108766

Physical Chemistry **Hot Paper**

Proton Traffic Jam: Effect of Nanoconfinement and Acid Concentration on Proton Hopping Mechanism

Ellen M. Adams[+], Hongxia Hao[+], Itai Leven, Maximilian Rüttermann, Hanna Wirtz, Martina Havenith, and Teresa Head-Gordon**

Abstract: *The properties of the water network in concentrated HCl acid pools in nanometer-sized reverse nonionic micelles were probed with TeraHertz absorption, dielectric relaxation spectroscopy, and reactive force field simulations capable of describing proton hopping mechanisms. We identify that only at a critical micelle size of $W_0 = 9$ do solvated proton complexes form in the water pool, accompanied by a change in mechanism from Grotthuss forward shuttling to one that favors local oscillatory hopping. This is due to a preference for H^+ and Cl^- ions to adsorb to the micelle interface, together with an acid concentration effect that causes a "traffic jam" in which the short-circuiting of the hydrogen-bonding motif of the hydronium ion decreases the forward hopping rate throughout the water interior even as the micelle size increases. These findings have implications for atmospheric chemistry, biochemical and biophysical environments, and energy materials, as transport of protons vital to these processes can be suppressed due to confinement, aggregation, and/or concentration.*

Introduction

Water within confined environments creates a perturbed hydrogen bonding network compared to the homogeneous bulk water phase, changing the electrostatic,[1] structural,[2] and dynamics[3] properties of the liquid. How confinement and interfaces alter solvated proton dynamics relative to the bulk phase is a critical factor in our understanding of important chemical and biological processes including proton transport at membrane surfaces,[4–6] for synthetic membranes used in fuel cells and separations,[7,8] and the acidic interfacial chemistry of aerosols, particularly those originating from marine environments.[9–12] In each case the chemistry or phase of the interfacial region and the dimensional constraints of the confinement can directly impact the water structure and dynamical transport mechanisms that can extend far from the surfaces themselves.

Fundamental studies of confined water dynamics have relied on the self-assembly of reverse micelles (RMs) in which the amphiphilic nature of surfactants in a nonpolar solvent organizes to encapsulate a water pool.[4,13–17] The surfactant headgroups of RMs can be changed to model charged or nonionic interfaces,[18–20] the chemical composition of the aqueous water pool can be altered to include salt and organic content,[21,22] and the size of the water pool can be easily tuned through the relation $W_0 = [H_2O]/[\text{surfactant}]$.[15,17] But in nearly all cases single particle and collective measures of water dynamics are found to be suppressed under confinement, including that of proton diffusion.[23,24] Seminal theoretical work from a number of research groups[5,25–31] have considered the mobility of a single solvated proton in bulk liquid water beyond the "structural diffusion" description put forward by Grotthuss.[32,33] A range of motion and timescales are operative,[34] including the fast and local oscillatory motions (proton rattling) as well as vehicular (Brownian motion) diffusion, but overall it is found to be dominated by the forward proton hopping mechanism through extended solvated hydronium complexes of the Eigen ($H_9O_4^+$) and Zundel ($H_5O_2^+$) motifs.[25–27] In the so-called "special partner dance"[26,34] the proton circulates through the 3 water molecules of the relatively long-lived Eigen complex, punctuated by favoring just one special pair partner that must

[*] Dr. E. M. Adams,[+] M. Rüttermann, Dr. H. Wirtz, Prof. M. Havenith
Lehrstuhl für Physkalische Chemie II, Ruhr Universität Bochum, 44801 Bochum (Germany)
E-mail: martina.havenith@ruhr-uni-bochum.de
Dr. H. Hao,[+] Dr. I. Leven, Prof. T. Head-Gordon
Chemical Sciences Division, Lawrence Berkeley National Laboratory, Berkeley, California 94720 (USA)
Dr. H. Hao,[+] Dr. I. Leven, Prof. T. Head-Gordon
Kenneth S. Pitzer Center for Theoretical Chemistry, University of California, Berkeley, California 94720 (USA)
E-mail: thg@berkeley.edu
Dr. H. Hao,[+] Dr. I. Leven, Prof. T. Head-Gordon
Department of Chemistry, University of California, Berkeley, California 94720 (USA)
Prof. T. Head-Gordon
Department of Chemical and Biomolecular Engineering, University of California, Berkeley, California 94720 (USA)
Prof. T. Head-Gordon
Department of Bioengineering, University of California, Berkeley, California 94720 (USA)
[+] These authors contributed equally to this work.
Supporting information and the ORCID identification number(s) for the author(s) of this article can be found under: https://doi.org/10.1002/anie.202108766.

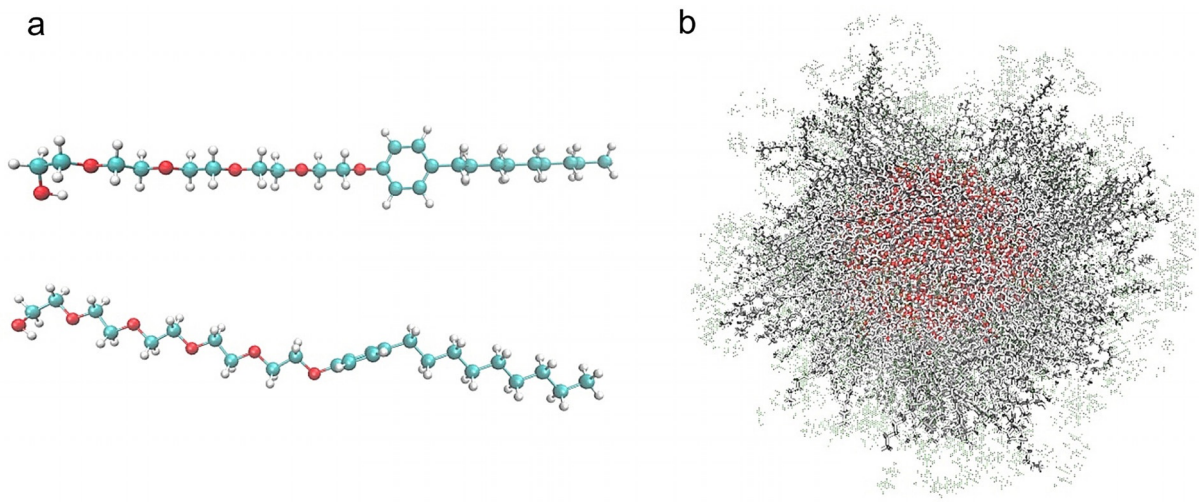

Figure 1. Structure of the nonionic surfactant IGEPAL CO-520. a) The reverse micelle surfactant is a polyether with a polar alcoholic group head group and a nonpolar chain incorporating an aromatic unit. b) The reverse micelle system with the pure water or HCl acidic pools encapsulated by the surfactants (in gray) and solvated in cyclohexane (in light green).

experience a reduction in coordination number to allow the proton charge defect to migrate,[34–37] while the coordination shell at the hydronium site is completed as it transfers the proton to a neighboring water.[28] Experimental studies using ultrafast vibrational[38] and 2D-IR spectroscopy[39–41] have emphasized the importance of Zundel structures as being a crucial configuration in proton transport on short timescales, but overall the low barrier to transformation between Eigen and Zundel states makes this structural distinction somewhat subtle, and may be better described as proton rattling between the two Eigen and Zundel extremes before a productive proton transfer occurs.[29,37,41]

Even so, the proton diffusion timescales and mechanisms can change under confinement as shown previously for water confined in reverse micelles composed of ionic[23] and nonionic[24] surfactants. Furthermore, many experimental studies of proton transport mechanisms have used concentrated acid solutions to create the source of hydronium ions.[42] While the effect of hydronium concentration on solvated proton dynamics have been investigated in bulk solution[43] it has not been thoroughly investigated under confinement using reverse micelles. Here we use a reactive force field, ReaxFF/C-GeM,[44,45] embedded in a non-reactive model of the nonionic surfactant IGEPAL CO-520 RM (Figure 1a), that together matches the experimental conditions of TeraHertz (THz) and dielectric relaxation (DR) spectroscopies as a function of HCl acid concentration and size of the reverse micelle (Figure 1b). THz spectroscopy is sensitive to the water network modes as well as to the solvated proton complex, and vibrational bands corresponding to the specific hydrated ions such as chloride have been identified.[46,47] The DR measurements allow us to estimate Debye relaxation timescales in different regions of the water pool and to provide a measure of conductivity in solution.

From these experiments we determine that there is near complete suppression of proton transport below a critical micelle size of $W_0 = 9$, while above this size solvated complexes of the proton form, along with a plateauing of DC conductance that we interpret as a stagnation in proton transfer rates even though the water pool is enlarged. Bolstered by the fact that our theoretical model shows excellent validation against these experiments we have discovered another explanation and counter-intuitive result that the Grotthuss proton hopping *decreases* with *increasing* RM size, and instead switches to a localized oscillatory hopping mechanism at and above the critical micelle size of $W_0 = 9$. This mechanistic change is due to an increase in the hydronium numbers that accumulate and stay at the interface with their Cl^- counter ion, and thus short-circuiting the hydrogen-bonded network through which protons hop over longer distances in 3D. Instead the 2D interfacial hydrogen-bonded network creates a "traffic jam" that shifts a majority of the protons to favor the localized oscillatory hopping mechanism as the RM size increases and/or as the acid concentration increases. The traffic jam refers to the obstruction to forward motion due to the loss of the full hydrogen-bonding motif of the hydrated Eigen complex arising from strong association with the polar interface.

Results

Previous studies have shown that only one water environment is present for smaller RMs, in which water molecules interact with the surfactant headgroup, that is, interfacial water, while for larger micelle sizes an inner core with more bulk-like water properties forms in addition to the interfacial water.[48,49] For the 1 M HCl acid solutions that are the source of protons, we have used THz-TDS and FTIR measurements to ascertain the properties of water in the presence of the dissociated ions Cl^- and H_3O^+ ions as a function of RM size.

The difference between the absorption spectra for RMs filled with pure water or 1 M HCl after subtraction of the absorption spectra of the minimum size reverse micelle

without any water ($W_0 = 0$ with only cyclohexane) [Equation (1)]:

$$\Delta\alpha_{W_{0,X}}(\nu, c) = \alpha_{W_{0,X}}(\nu, c) - \alpha_{W_0}(\nu, c) \quad (1)$$

are reported in Figure 2a and b as a function of increasing RM size from $W_{0,X} = 1$ to $W_{0,X} = 20$ where ν is the frequency and c is the water concentration. It is seen that the THz-TDS (10–100 cm^{-1}) and FTIR (100–400 cm^{-1}) data fit together seamlessly, with $\Delta\alpha_{W_{0,X}}(\nu, c)$ increasing over the measured frequency range and dominated by a vibrational band at ca. 200 cm^{-1} assigned to the intermolecular hydrogen bonding stretch of water.[50] An increase in the absorption with increasing micelle size is also observed, consistent with a larger volume fraction of water present inside the micelle, a feature that has been observed for other RM systems.[16,51,52] We note that values of $\Delta\alpha$ for the 1 M HCl RMs are similar to that of the pure water RMs (Figure S1 in Supporting Information). This result is surprising as measurements of a bulk 1 M HCl solution found an increase in absorption relative to bulk water of at least $\approx 30\ cm^{-1}$ in the same frequency range.[46,53]

This therefore indicates that dissociated acid molecules in the nanoconfined RM environment are not solvated in the same manner as in bulk solution.[54–56] Previous studies with NMR by the Levinger group observed similar results, in which it was determined that an NMR probe freely tumbled within the bulk-like core of IGEPAL CO-520 RMs, but that the pH within the RM core was less acidic than the bulk solution from which the RMs were prepared,[57] and indicates that confinement of the acidic solution may impact the pKa or distribution of acid molecules.

To isolate the THz signatures of the hydrated hydronium and chloride ions more directly, Figure 2c shows the double difference spectra $\Delta\Delta\alpha(\nu, c)$ for select RM sizes, determined by subtracting $\Delta\alpha_X(\nu, c)$ of the reverse micelles filled with pure water from $\Delta\alpha_X(\nu, c)$ of the same RM size with a 1 M HCl acid solution [Equation (2)]:

$$\Delta\Delta\alpha_{W_{0,X}}(\nu, c) = \Delta\alpha_{W_0(1\ M\ HCl)}(\nu, c) - \Delta\alpha_{W_0(0\ M\ HCl)}(\nu, c) \quad (2)$$

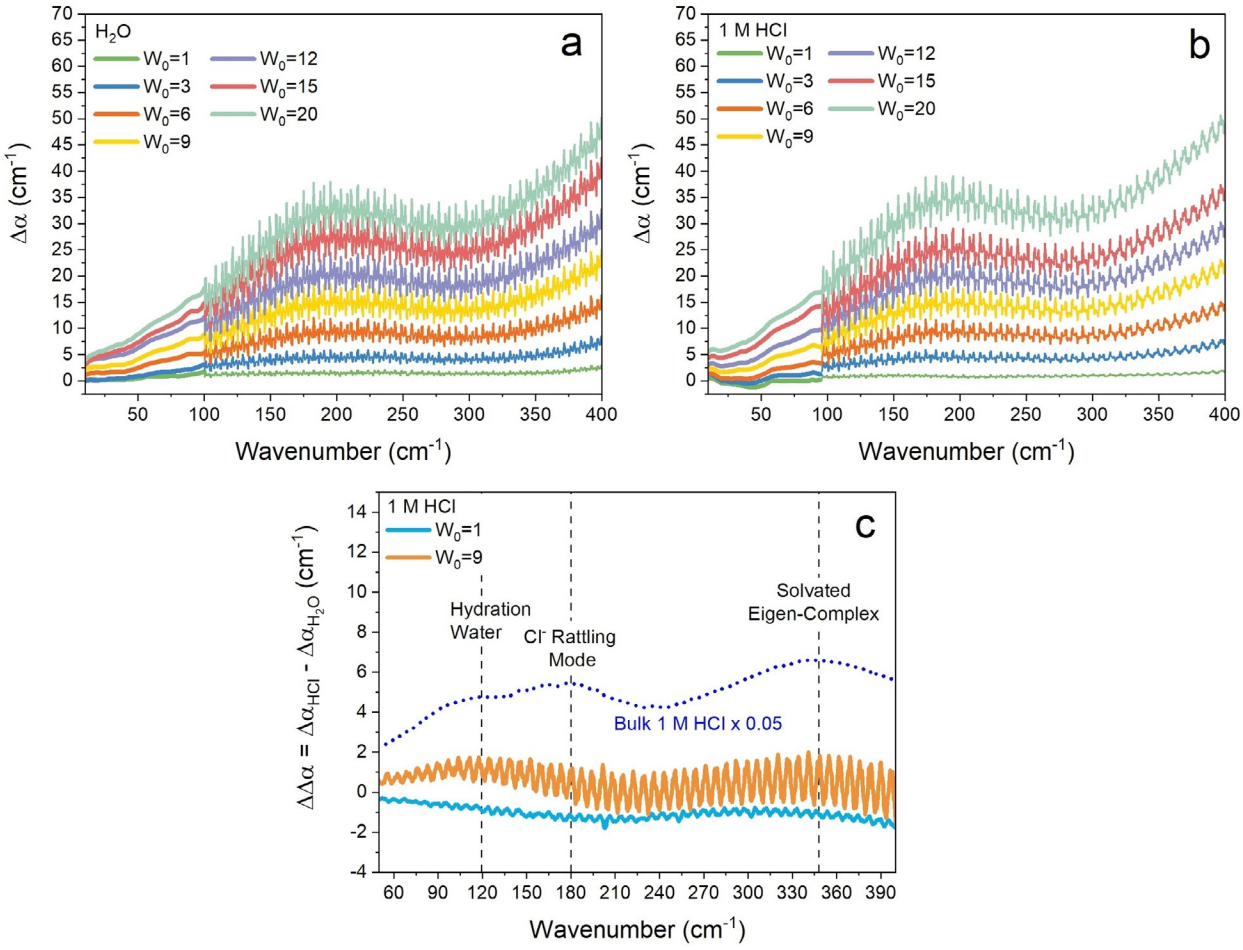

Figure 2. THz-TDS and FTIR absorption spectra for pure water and HCl solutions as a function of reverse micelle size. The difference absorption spectra $\Delta\alpha_X(\nu, c)$ for RMs filled with a) water and b) 1 M HCl after subtraction of $W_0 = 0$. Below 100 cm^{-1} spectra were collected with THz-TDS with an average error of 0.6 cm^{-1}. Above 100 cm^{-1} spectra were collected with THz-FTIR with an average error of 5 cm^{-1}. c) The double difference absorption spectra, $\Delta\Delta\alpha(\nu, c)$, for 1 M HCl acid solutions, determined by subtracting the reverse micelles of the same size filled with pure water. The reverse micelles exhibit vibrational bands corresponding to hydration water (120–150 cm^{-1}), the solvated Eigen-complex (360 cm^{-1}) and the vibrational band corresponding to the Cl^- rattling mode in bulk 1 M HCl solution (180 cm^{-1}). Since the 180 cm^{-1} mode is missing in the acidic RMs, it indicates the Cl^- ions are adsorbed at the micelle surface.

This is the spectral difference between a RM confined HCl solution versus a RM confined neat water pool. For $W_0 = 1$, $\Delta\Delta\alpha_{W0,X}(\nu, c)$ is close to 0 cm^{-1}, however at $W_0 = 9$ two bands appear at approximately 120 and 360 cm^{-1} (which are more evident at higher acid concentrations given in Figure S2). Previous measurements of aqueous bulk HCl solutions (blue dashed line in Figure 2c) attribute the 120 cm^{-1} band to modes related to hydration water, and the band at 360 cm^{-1} to a "rattling" mode of the solvated Eigen complex.[46] Bulk 1 M HCl solution measurements also observed another band at 180 cm^{-1} which was assigned to the Cl^- rattling mode (see Figure S3 for the spectral deconvolution of bulk 1 M HCl spectrum) based on comprehensive measurements of Cl^- salts as well as simulations.[47,58,59] This mode is noticeably absent in the RM spectra for the 1 M HCl data at all sizes (Figure 2c and Figure S2), which suggests that Cl^- ions preferentially adsorb to the surfactant headgroup and stripping off of the hydration shell. In totality, these measurements indicate that the chloride ions are adsorbed to the surface and that a solvated proton complex undergoing a rattling motion forms in the RM at 1 M HCl, but only when the size restriction of $W_0 = 6$ is overcome (Figure S2). Although not directly comparable, similar size constraint effects were observed in studies by Levinger, in which tumbling of the NMR probe was restricted for $W_0 = 5$ compared to larger sizes.[57] Furthermore, a recent study from Sofronov and Bakker also showed a lack of anisotropy decay for cationic RMs with radii < 2 nm (nearly the same size as $W_0 = 6$).[23] This size dependent effect could point a change in the distribution of water within the RMs (from interfacial to bulk or non-uniform to uniform) that subsequently impacts proton hydration and transport.[60]

Figure 3 shows the real (ε') and imaginary (ε'') parts of the relative permittivity from DR experiments of water-filled and 1 M HCl solutions in the reverse micelles. Results of water-only RMs are consistent with those previously reported, in which a feature appears in the ε'' spectra that grows in intensity and shifts to higher frequency with increasing micelle size.[51,61] But the ε' and ε'' spectra of the 1 M HCl RMs differs drastically from those of water RMs, in which a sudden increase in the ε'' spectra occurs starting at $W_0 = 9$ for low frequencies. This is consistent with a Drude-Lorentz mode at zero frequency: for $\nu \to 0$, the dielectric spectrum of an electrolyte is dominated by the so-called conduction band, that is, an additional term: $\frac{\sigma_{DC}}{\varepsilon_0 \omega}$ with σ_{DC} providing a measure for the conductivity. This rapid onset shows that conductance in the solution due to the HCl molecules does not occur for micelle sizes smaller than $W_0 = 9$ but is activated above that

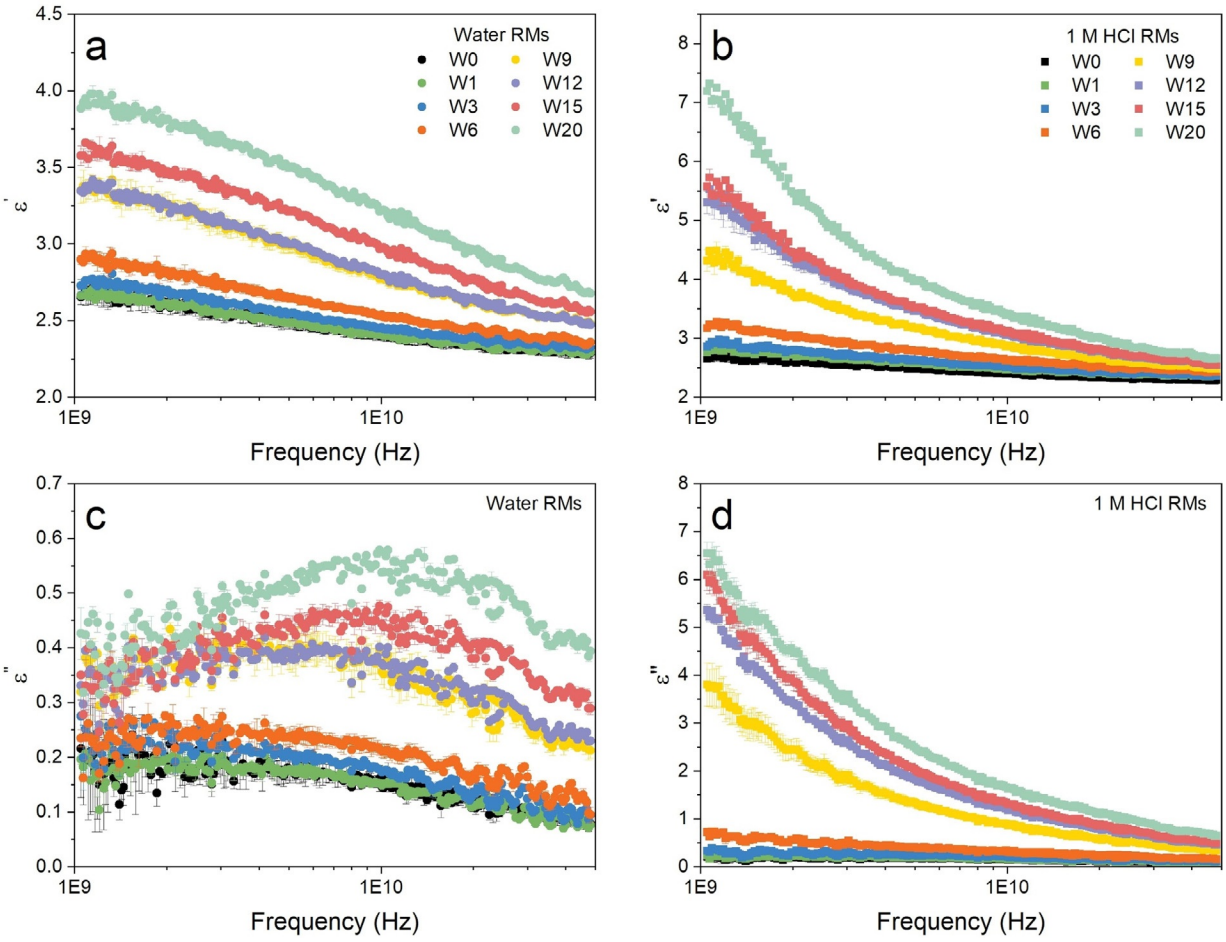

Figure 3. Real and imaginary components of the dielectric permittivity of reverse micelles containing water and 1 M HCl acid solution. The real part ε' for RMs containing a) pure water and b) 1 M HCl. The imaginary part ε'' for c) pure water and d) 1 M HCl.

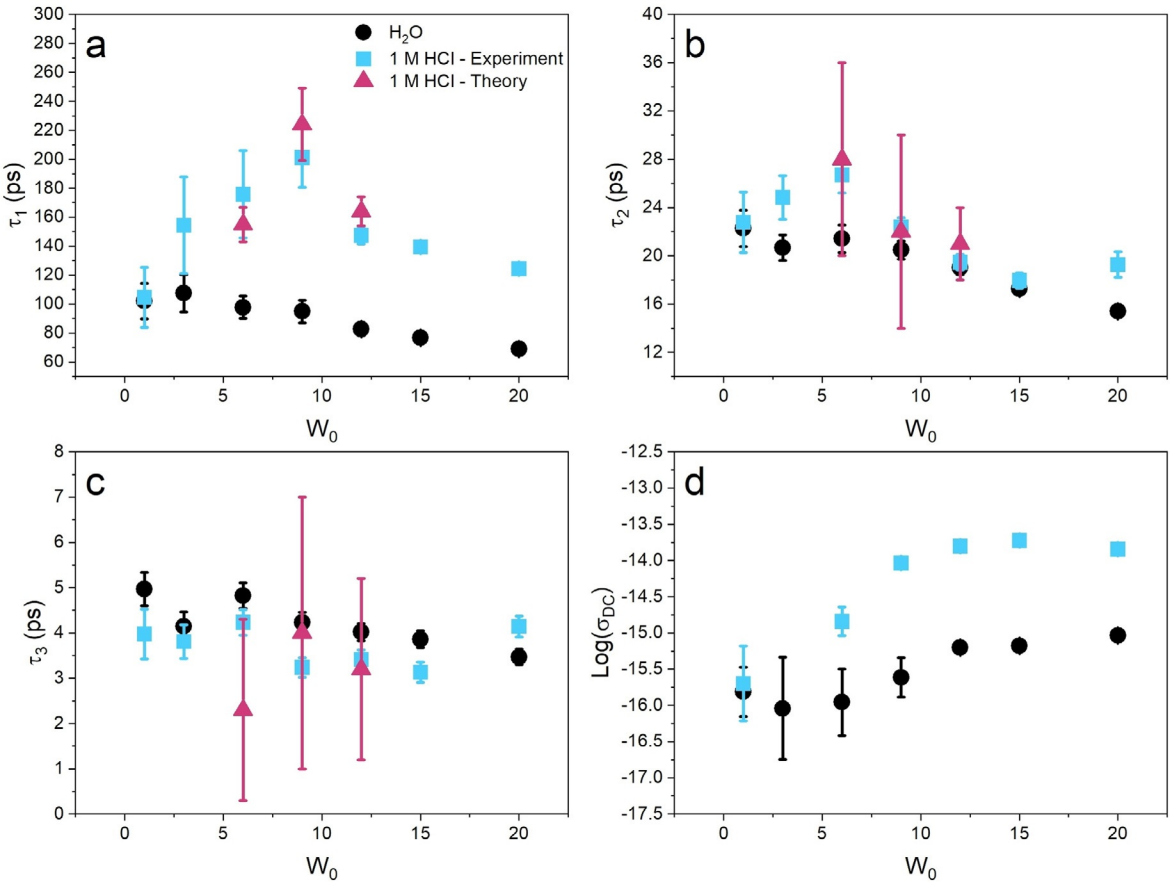

Figure 4. Rotational relaxation time constants and conductance determined for reverse micelles containing water and 1 M HCl acid solution. Simultaneous fitting of the real and imaginary parts of the dielectric response yield Debye relaxation times for a) interfacial water (τ_1), b) slow core water (τ_2), c) fast core water (τ_3), and d) conductance (σ_{DC}). Further details are provided in Methods and the numerical results of the fits can be found in Supplementary Tables S1, S2 and S3.

size. The complex relative permittivity, $\varepsilon(\omega)=\varepsilon'-i\varepsilon''$, of the RM data can then be modeled as a sum of three Debye modes representing contributions from interfacial water and bulk-like core water in addition to the conductivity term[62] [Equation (3)]:

$$\varepsilon(\omega)=\varepsilon_\infty+\sum_i^3\frac{\Delta\varepsilon_i}{1+i\omega 2\pi\tau_i}+\frac{\sigma_{DC}}{\varepsilon_0\omega} \tag{3}$$

where ε_∞ is the relative permittivity at the high frequency limit, $\Delta\varepsilon_i$ is the permittivity amplitude, τ_i is the relaxation time constant of each component.

Figure 4a–c shows the time constants determined from fitting for the pure water and 1 M HCl reverse micelles. Here τ_1 represents the reorientation timescale of interfacial water, while τ_2 and τ_3 represent the slow and fast reorientation processes of the pure water or HCl solution in the core. Results for the pure water RMs reported here exhibit an interfacial water timescale of 100 ps for $W_0=1$ and decreases to 70 ps for $W_0=20$ (Figure 4a), and the slow reorientation timescale of core water τ_2 decreases from 22 to 15 ps while the fast reorientation core water τ_3 similarly decreases from 5 to 3 ps with increasing micelle size (Figure 4b and c), all consistent with previous studies.[13,16,18,61,63] The amplitude of the conductance band at all reverse micelle sizes is suppressed relative to bulk water values, but systematically increases as reverse micelle size increases (Figure 4d).

While the slow and fast reorientation timescale τ_2 and τ_3 of core water in the 1 M HCl acid pools shows similar timescales to the pure water pool, the interfacial water τ_1 time constant is slowed by up to a factor of 2 compared to the pure water pools regardless of RM size (Figure 4a–c). This observation concerning the interfacial time constant τ_1, together with the THz measurements, support the fact that both hydronium and chloride accumulate at the interface. This is consistent with theoretical studies by Li and Voth[24] and experiments using surface specific sum frequency generation that have also revealed that Cl^- and H_3O^+ ions have an equal preference to be found at the interface for alcohol-terminated monolayers.[64] With increasing RM size in the presence of HCl we observe a much larger value for the conductance than confined pure water, consistent with greater numbers of protons, but the conductance plateaus once the critical size of $W_0=9$ is reached (Figure 4d). Dielectric spectra of IGEPAL CO-520 RMs filled with 1 M NaCl were also measured and show no increase in the real or imaginary component of the permittivity with increasing micelle size (Figure S4). This establishes that the changes in the relaxation

times and increase in conductivity is unique for the 1 M HCl solution, and by inference the proton complexes in solution. It is also possible that changes in pH can also affect proton transfer in which lower dielectric constant media have been shown to concomitantly reduce the proton transfer rates[65] or that nanoconfinement itself could impact that fraction of dissociated HCl molecules in solution relative to the bulk solution, thereby altering the local pH. What the exact pH in RMs is has been a long outstanding question in this field, and previous studies from the Crans and Levinger groups have attempted to answer this question for both ionic and nonionic reverse micelles.[4] They determined that the pH inside of IGEPAL CO-520 RMs of sizes $W_0 = 5$ to 15 tends toward a neutral pH in the micelle core, and in general that the RM environment is always less acidic than bulk as a function of hydronium concentration. This is especially true for the RM system studied here since the hydronium segregates more to the interface leaving the interior water pH less acidic than the same HCl concentration as the unconfined system.

Taken altogether, the experimental results show that the solvated proton dynamics is inhibited for acidic water in micelles smaller than $W_0 = 9$ due to confinement effects similar to that of pure water, while above this critical RM size the conductance plateaus at the same point in which the rattling mode emerges from the THz measurements. We have sought to unravel the underlying solvated proton mechanism in the THz and DR experiments by performing molecular dynamics simulations with a hybrid model where the same IGEPAL CO-520 surfactant that self-assembles in cyclohexane is described with a classical force field and the water pool with or without HCl is described by the ReaxFF-CGeM model as a function of the same RM size used in the experiment. The ReaxFF-CGeM reactive force field allows us to represent hydronium complexes of the Eigen and Zundel motifs (Figure 5a and Figure S5)[44,45] and to evaluate the cross-over of large and concentrated acidic pools which is not accessible to other AIMD and multistate empirical valence bond (MS-EVB) methodology. The ReaxFF-CGeM water model has been shown to yield good quantitative agreement

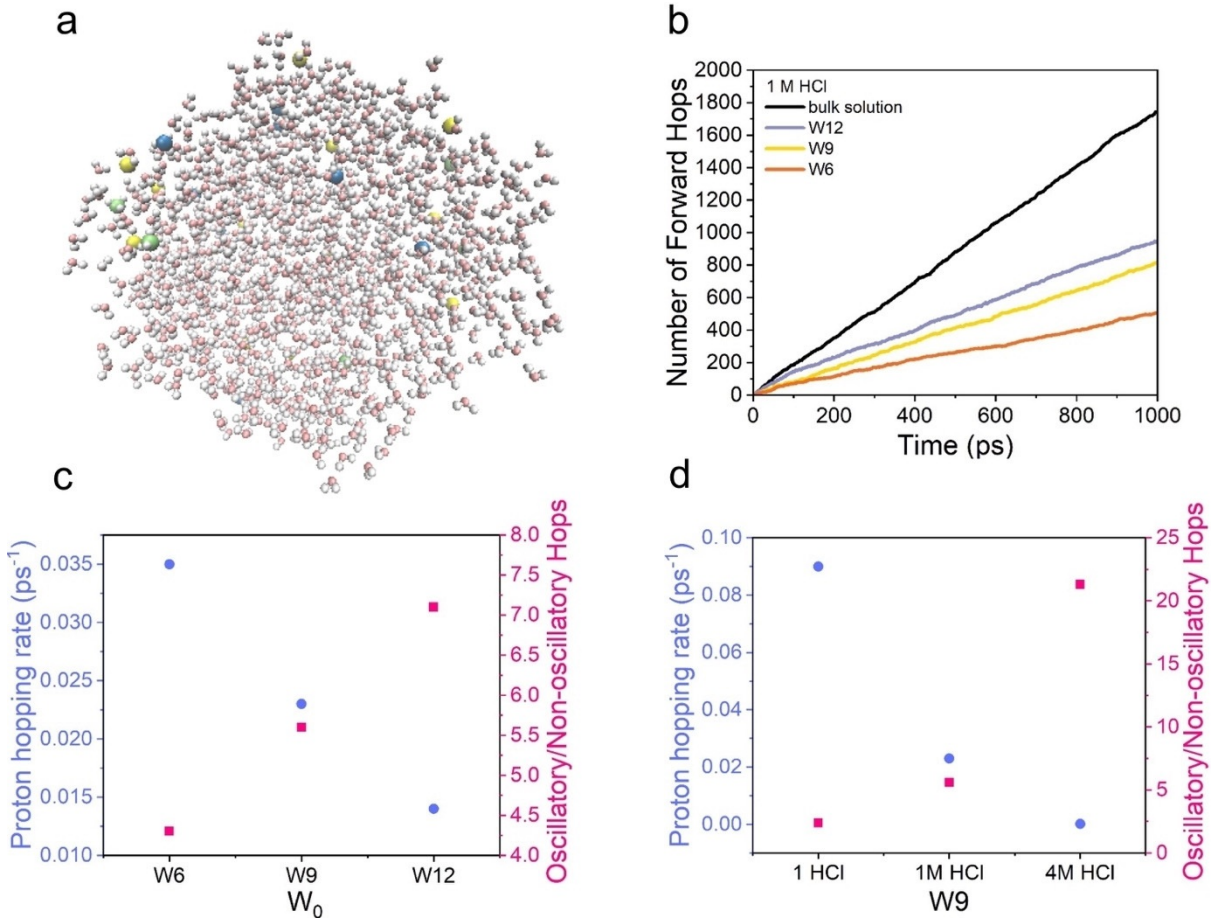

Figure 5. Molecular dynamics simulation of the pure and HCl water pools in IGEPAL reverse micelles using ReaxFF/C-GeM. a) The cross-section depiction of the HCl acid water pool showing that the Cl ions (gold), Eigen-like hydronium in green, Zundel-like hydronium in blue are largely seen to be distributed at the RM interface. b) Number of forward proton hops (without oscillatory motion) calculated from an MD trajectory from each RM system and a bulk water system with 1 M HCl solution. c) Proton hopping rates per hydronium (blue dot) and ratio of oscillatory to non-oscillatory hops (red square) calculated from an MD trajectory from each 1 M HCl reverse micelle system. d) Proton hopping rates per hydronium (blue dot) and ratio of oscillatory to non-oscillatory hops (red square) calculated from an MD trajectory from $W_0 = 9$ reverse micelle system of varying HCl concentration. The full results can be found in Supplementary Figure S5 and Table S4.

for bulk water structure, thermodynamic, and transport properties, including hydronium and hydroxide diffusion rates,[44] while also predicting the contact and solvent ion pair for chloride in water.[45]

Because $W_0 = 9$ serves as a transition point in the experiments, we characterized the pure water and acid pools from $W_0 = 6$ to $W_0 = 12$. Figure 4a–c shows that the simulated DR rotational timescales match the magnitude of the three experimental time scales very well for the 1 M HCl RM. Like that inferred from the THz and DR experimental data, the Cl^- and solvated H_3O^+ ions accumulate strongly at the interface for the acid pools (Figures 5a and Figure S6. Figure 5b shows that the forward proton hopping number increases significantly between $W_0 = 6$ and $W_0 = 9$, but then increases by only $\approx 10\,\%$ between $W_0 = 9$ and $W_0 = 12$ for the acid containing RMs. We equate the forward hopping mechanism to directional flow of charge as the proton travels over larger distances, which is found to diminish with increasing RM size, and thus is consistent with the experimental measure of DC conductance that plateaus above the critical $W_0 = 9$ RM size in the 1 M HCl case. Altogether the theoretical results are well-validated against the experimental data and confirms our ability to interpret the proton hopping mechanism as a function of RM size and acid concentration.

Two types of proton mechanistic hopping events were considered: (1) oscillatory shuttling or "rattling" where the proton hops back and forth between the hydronium cation and an adjacent water molecule, and (2) forward hopping where the proton hops to a second and then onto a third water molecule instead of hopping back to its donor. When evaluating the proton hopping rate constant we find that it continually slows as the RM size increases, even though the inner core of these RMs are large enough to have bulk-like dynamics (blue symbols in Figure 5c), and the more, minor oscillatory mechanism found in pure water becomes the major mechanism in HCl acid pools in reverse micelles (red symbols in Figure 5c). In Figure 5d we consider the effect of HCl concentration by going as low as 1 HCl molecule to a large concentration of 4 M HCl. As might be expected the single HCl molecule is dominated by the forward hopping mechanism, and represents that expected in pure water pools, whereas the oscillatory mechanism becomes even more pronounced at 4 M concentrations relative to the 1 M case. This is consistent with that of the Bakker group that also demonstrated a retardation of proton hopping by a factor of 4 in cationic RMs filled with 4–7 M HBr with anisotropy measurements, even at larger RM sizes.[23] Interestingly the cross-over in proton hopping mechanism occurs at the critical RM size of $W_0 = 9$ and at 1 M HCl concentration.

Figure 6 provides an explanation for the observations of the switch in mechanism from forward to oscillatory hopping at $W_0 = 9$ found from the simulations. When we evaluate the pairings of a central hydronium ion undergoing oscillatory hopping with 1 M HCl we find an increase from $W_0 = 6$ to $W_0 = 9$ to $W_0 = 12$ in which a regular water molecule is substituted for a surfactant head group, or even a chloride or other hydronium, unlike hydroniums that undergo forward hopping that show a reduction in substitution as RM size increases. The increase in the 1st solvation shell substitution as RM size increases in the presence of acid induces an increase in the Zundel motif ($\delta = 0.2$) for the remaining complexed waters of the Eigen complex (Figure 6 and Table S6), but remains unproductive as a forward hopping intermediate or transition state as it is in bulk water.[37,41,66] This is especially dramatic as acid concentration increases (Table S7).

Conclusion

We have determined that the slowing of the overall forward hopping rate is attributable to a localized concentration effect of hydronium and chloride ions at the water-surfactant interface, creating a traffic jam of protons unable to execute Grotthuss shuttling as the 2D hydrogen bonded network decreases its capacity for free and better percolated pathways at the RM interface (supported in Table S5), unlike that found at the air–water interface.[68,69] The water network in acidic nanometer-sized reverse micelles have been probed with both THz absorption and dielectric relaxation spectroscopies, identifying a critical reverse micelle size of $W_0 = 9$ in which the Eigen hydronium complex is evident while at the same time the interfacial water dynamics slows considerably relative to pure water containing reverse micelles. Reactive molecular dynamics simulations show excellent agreement

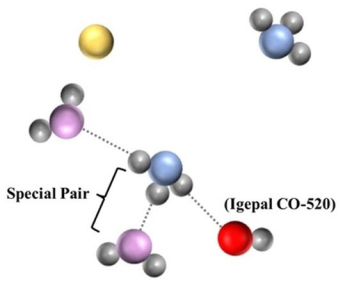

Substitutions of the Eigen complex	Forward hydroniums				Oscillatory hydroniums		
	W6	W9	W12		W6	W9	W12
H_3O^+-H_3O^+	1.0	3.0	5.0		1.0	3.0	4.0
H_3O^+-Cl^-	4.0	4.0	3.0		5.0	11.0	12.0
H_3O^+-surfactant	15.0	15.0	9.4		29.0	22.7	27.0
Zundel complex			W6	W9	W12		
			0.8	12.0	26.0		

Figure 6. Alterations in the 1st shell solvation structure of the hydronium ion in 1 M HCl reverse micelles induces an increase in the Zundel motif. The Eigen complex with a central hydronium oxygen (blue) pairs with not only other water molecules (pink) but shows increases in substitutions with surfactant oxygens (red), chloride (gold), and other hydronium ions. The pairings are defined by the 1st solvation shell defined by the radial distribution function. As the substituted pairings increase, we see an increase in Zundel structures ($\delta < 0.2$ for Zundel and otherwise for Eigen[67]) with the other water molecules.

with these experimental measurements and have been used to characterize the proton hopping mechanism as a function of RM size and HCl acid concentration. We have shown that for either smaller RMs and/or weaker acid concentrations the forward hopping mechanism dominates, whereas for larger RMs and larger acid concentrations the proton rattling motion is preferred. This effect arises from the strong co-adsorption of hydronium to the interface with its chloride counter ion with increasing acid concentration, which creates a minimal amount of water solvation in a 2D interfacial network with a reduced hydrogen-bonding capacity.[69] In fact only recently has evidence of the hydration structure of protons at an interface been observed, where Eigen-like hydrated protons ($H_9O_4^+$) were identified near negatively charged monolayers at biologically relevant pH,[70] similar to the observations made here.

We have shown that a consequence of this interfacial chemistry is that it creates a proton traffic jam that is unable to fulfill forward hopping into the larger water pools as the RM size increases. In particular the interfacial substitutions of water for other species (surfactants, chlorides, and other hydroniums) induces changes in the other water molecules complexed to a central hydronium with increases in "Zundel" formation as the proton oscillates between the two molecules. These findings have significant implications for deeper understanding of many applications where transport of protons is necessary for function. For instance, studies of aerosols have found that pH is linked to the particle size,[10,71] and thus influences the chemical reactivity, hygroscopicity, and ability of aerosol particles to act as ice and cloud condensation nuclei.[72–74] The Grotthuss mechanism of proton is thought to be the main method of proton transport at biological membrane surfaces,[5] but as we have shown can change to a localized oscillatory hopping if proton concentration is high enough, an aspect of biological signaling that deserves further investigation.

Acknowledgements

This research was supported under Germany's Excellence Strategy—EXC 1069 and EXC 2033—Projektnummer 390677874 from the *Deutsche Forschungsgemeinschaft* (DFG, German Research Foundation) via the Cluster of Excellence RESOLV, and the Research Training Group "Confinement-controlled Chemistry" under Grant GRK2376-331085229 from the DFG. H.H. and T.H.G. were supported under the CPIMS program by the Director, Office of Science, Office of Basic Energy Sciences, Chemical Sciences Division of the U.S. Department of Energy under Contract No. DE-AC02-05CH11231. This research used resources of the National Energy Research Scientific Computing Center, a DOE Office of Science User Facility supported by the Office of Science of the U.S. Department of Energy under Contract No. DE-AC02-05CH11231. Open Access funding enabled and organized by Projekt DEAL.

Conflict of Interest

The authors declare no conflict of interest.

Keywords: confined water · Grotthuss mechanism · micelles · proton hopping · THz spectroscopy

[1] F. Jiménez-Ángeles, K. J. Harmon, T. D. Nguyen, P. Fenter, M. Olvera de la Cruz, *Phys. Rev. Res.* **2020**, *2*, 043244.
[2] L. Ruiz Pestana, L. E. Felberg, T. Head-Gordon, *ACS Nano* **2018**, *12*, 448–454.
[3] M.-C. Bellissent-Funel, *Eur. Phys. J. E* **2003**, *12*, 83–92.
[4] D. C. Crans, N. E. Levinger, *Acc. Chem. Res.* **2012**, *45*, 1637–1645.
[5] N. Agmon, H. J. Bakker, R. K. Campen, R. H. Henchman, P. Pohl, S. Roke, M. Thämer, A. Hassanali, *Chem. Rev.* **2016**, *116*, 7642–7672.
[6] F. Giberti, A. A. Hassanali, *J. Chem. Phys.* **2017**, *146*, 244703.
[7] S. Das, S. Imoto, S. Sun, Y. Nagata, E. H. G. Backus, M. Bonn, *J. Am. Chem. Soc.* **2020**, *142*, 945–952.
[8] X. Ling, M. Bonn, K. F. Domke, S. H. Parekh, *Proc. Natl. Acad. Sci. USA* **2019**, *116*, 8715–8720.
[9] E. M. Knipping, *Science* **2000**, *288*, 301–306.
[10] W. C. Keene, *Geophys. Res. Lett.* **2002**, *29*, 1101.
[11] Y. Li, M. J. Ezell, B. J. Finlayson-Pitts, *Atmos. Environ.* **2011**, *45*, 4123–4132.
[12] H. O. T. Pye, A. Nenes, B. Alexander, A. P. Ault, M. C. Barth, S. L. Clegg, J. L. Collett, Jr., K. M. Fahey, C. J. Hennigan, H. Herrmann, M. Kanakidou, J. T. Kelly, I.-T. Ku, V. F. McNeill, N. Riemer, T. Schaefer, G. Shi, A. Tilgner, J. T. Walker, T. Wang, R. Weber, J. Xing, R. A. Zaveri, A. Zuend, *The Acidity of Atmospheric Particles and Clouds*, Aerosols/Atmospheric Modelling/Troposphere/Chemistry (Chemical Composition And Reactions), **2019**.
[13] D. E. Moilanen, N. E. Levinger, D. B. Spry, M. D. Fayer, *J. Am. Chem. Soc.* **2007**, *129*, 14311–14318.
[14] B. Baruah, D. C. Crans, N. E. Levinger, *Langmuir* **2007**, *23*, 6510–6518.
[15] M. D. Fayer, N. E. Levinger, *Annu. Rev. Anal. Chem.* **2010**, *3*, 89–107.
[16] T. H. van der Loop, M. R. Panman, S. Lotze, J. Zhang, T. Vad, H. J. Bakker, W. F. C. Sager, S. Woutersen, *J. Chem. Phys.* **2012**, *137*, 044503.
[17] D. Laage, T. Elsaesser, J. T. Hynes, *Chem. Rev.* **2017**, *117*, 10694–10725.
[18] E. E. Fenn, D. B. Wong, M. D. Fayer, *Proc. Natl. Acad. Sci. USA* **2009**, *106*, 15243–15248.
[19] R. Costard, N. E. Levinger, E. T. J. Nibbering, T. Elsaesser, *J. Phys. Chem. B* **2012**, *116*, 5752–5759.
[20] A. Phukon, S. Ray, K. Sahu, *Langmuir* **2016**, *32*, 10659–10667.
[21] K. J. Blackshaw, M. G. Varmecky, J. D. Patterson, *J. Phys. Chem. A* **2019**, *123*, 336–342.
[22] D. S. Venables, K. Huang, C. A. Schmuttenmaer, *J. Phys. Chem. B* **2001**, *105*, 9132–9138.
[23] O. O. Sofronov, H. J. Bakker, *ACS Cent. Sci.* **2020**, *6*, 1150–1158.
[24] Z. Li, G. A. Voth, *Phys. Chem. Chem. Phys.* **2020**, *22*, 10753–10763.
[25] U. W. Schmitt, G. A. Voth, *J. Chem. Phys.* **1999**, *111*, 9361–9381.
[26] D. Marx, M. E. Tuckerman, J. Hutter, M. Parrinello, *Nature* **1999**, *397*, 601–604.
[27] R. Vuilleumier, D. Borgis, *J. Chem. Phys.* **1999**, *111*, 4251–4266.
[28] T. C. Berkelbach, H.-S. Lee, M. E. Tuckerman, *Phys. Rev. Lett.* **2009**, *103*, 238302.
[29] D. Marx, A. Chandra, M. E. Tuckerman, *Chem. Rev.* **2010**, *110*, 2174–2216.

[30] A. Hassanali, F. Giberti, J. Cuny, T. D. Kühne, M. Parrinello, *Proc. Natl. Acad. Sci. USA* **2013**, *110*, 13723 – 13728.
[31] E. Codorniu-Hernández, P. G. Kusalik, *Proc. Natl. Acad. Sci. USA* **2013**, *110*, 13697 – 13698.
[32] C. J. T. de Grotthuss, *Ann. Chim.* **1806**, *LVIII*, 54 – 74.
[33] N. Agmon, *Chem. Phys. Lett.* **1995**, *244*, 456 – 462.
[34] C. Knight, G. A. Voth, *Acc. Chem. Res.* **2012**, *45*, 101 – 109.
[35] M. Tuckerman, K. Laasonen, M. Sprik, M. Parrinello, *J. Chem. Phys.* **1995**, *103*, 150 – 161.
[36] M. Tuckerman, K. Laasonen, M. Sprik, M. Parrinello, *J. Phys. Chem.* **1995**, *99*, 5749 – 5752.
[37] C. Li, J. M. J. Swanson, *J. Phys. Chem. B* **2020**, *124*, 5696 – 5708.
[38] S. Woutersen, H. J. Bakker, *Phys. Rev. Lett.* **2006**, *96*, 138305.
[39] F. Dahms, R. Costard, E. Pines, B. P. Fingerhut, E. T. J. Nibbering, T. Elsaesser, *Angew. Chem. Int. Ed.* **2016**, *55*, 10600 – 10605; *Angew. Chem.* **2016**, *128*, 10758 – 10763.
[40] F. Dahms, B. P. Fingerhut, E. T. J. Nibbering, E. Pines, T. Elsaesser, *Science* **2017**, *357*, 491 – 495.
[41] M. Thämer, L. De Marco, K. Ramasesha, A. Mandal, A. Tokmakoff, *Science* **2015**, *350*, 78 – 82.
[42] R. Yuan, J. A. Napoli, C. Yan, O. Marsalek, T. E. Markland, M. D. Fayer, *ACS Cent. Sci.* **2019**, *5*, 1269 – 1277.
[43] J. Xu, S. Izvekov, G. A. Voth, *J. Phys. Chem. B* **2010**, *114*, 9555 – 9562.
[44] I. Leven, H. Hao, A. K. Das, T. Head-Gordon, *J. Phys. Chem. Lett.* **2020**, *11*, 9240 – 9247.
[45] I. Leven, T. Head-Gordon, *J. Phys. Chem. Lett.* **2019**, *10*, 6820 – 6826.
[46] D. Decka, G. Schwaab, M. Havenith, *Phys. Chem. Chem. Phys.* **2015**, *17*, 11898 – 11907.
[47] G. Schwaab, F. Sebastiani, M. Havenith, *Angew. Chem. Int. Ed.* **2019**, *58*, 3000 – 3013; *Angew. Chem.* **2019**, *131*, 3030 – 3044.
[48] J. Chowdhary, B. M. Ladanyi, *J. Phys. Chem. B* **2009**, *113*, 15029 – 15039.
[49] D. E. Moilanen, E. E. Fenn, D. Wong, M. D. Fayer, *J. Chem. Phys.* **2009**, *131*, 014704.
[50] M. Heyden, M. Havenith, *Methods* **2010**, *52*, 74 – 83.
[51] A. Patra, T. Q. Luong, R. K. Mitra, M. Havenith, *Phys. Chem. Chem. Phys.* **2013**, *15*, 930 – 939.
[52] A. Patra, T. Q. Luong, R. K. Mitra, M. Havenith, *Phys. Chem. Chem. Phys.* **2014**, *16*, 12875.
[53] O. F. Mohammed, D. Pines, J. Dreyer, E. Pines, E. T. J. Nibbering, *Science* **2005**, *310*, 83 – 86.
[54] P. Jungwirth, D. J. Tobias, *J. Phys. Chem. B* **2002**, *106*, 6361 – 6373.
[55] C. Tian, N. Ji, G. A. Waychunas, Y. R. Shen, *J. Am. Chem. Soc.* **2008**, *130*, 13033 – 13039.
[56] I. Gladich, P. B. Shepson, M. A. Carignano, I. Szleifer, *J. Phys. Chem. A* **2011**, *115*, 5895 – 5899.
[57] M. A. Sedgwick, D. C. Crans, N. E. Levinger, *Langmuir* **2009**, *25*, 5496 – 5503.
[58] S. Funkner, G. Niehues, D. A. Schmidt, M. Heyden, G. Schwaab, K. M. Callahan, D. J. Tobias, M. Havenith, *J. Am. Chem. Soc.* **2012**, *134*, 1030 – 1035.
[59] P. Schienbein, G. Schwaab, H. Forbert, M. Havenith, D. Marx, *J. Phys. Chem. Lett.* **2017**, *8*, 2373 – 2380.
[60] T. Zelovich, K. I. Winey, M. E. Tuckerman, *J. Mater. Chem. A* **2021**, *9*, 2448 – 2458.
[61] T. H. van der Loop, N. Ottosson, S. Lotze, E. Kentzinger, T. Vad, W. F. C. Sager, H. J. Bakker, S. Woutersen, *J. Chem. Phys.* **2014**, *141*, 18C535.
[62] M. Senske, Y. Xu, A. Bäumer, S. Schäfer, H. Wirtz, J. Savolainen, H. Weingärtner, M. Havenith, *Phys. Chem. Chem. Phys.* **2018**, *20*, 8515 – 8522.
[63] S. Park, D. E. Moilanen, M. D. Fayer, *J. Phys. Chem. B* **2008**, *112*, 5279 – 5290.
[64] Y.-C. Wen, S. Zha, C. Tian, Y. R. Shen, *J. Phys. Chem. C* **2016**, *120*, 15224 – 15229.
[65] M. Ekimova, F. Hoffmann, G. Bekçioğlu-Neff, A. Rafferty, O. Kornilov, E. T. J. Nibbering, D. Sebastiani, *J. Am. Chem. Soc.* **2019**, *141*, 14581 – 14592.
[66] W. B. Carpenter, J. A. Fournier, N. H. C. Lewis, A. Tokmakoff, *J. Phys. Chem. B* **2018**, *122*, 2792 – 2802.
[67] D. Marx, *ChemPhysChem* **2006**, *7*, 1848 – 1870.
[68] S. Pezzotti, D. R. Galimberti, M.-P. Gaigeot, *J. Phys. Chem. Lett.* **2017**, *8*, 3133 – 3141.
[69] S. Pezzotti, A. Serva, M.-P. Gaigeot, *J. Chem. Phys.* **2018**, *148*, 174701.
[70] E. Tyrode, S. Sengupta, A. Sthoer, *Nat. Commun.* **2020**, *11*, 493.
[71] R. L. Craig, P. K. Peterson, L. Nandy, Z. Lei, M. A. Hossain, S. Camarena, R. A. Dodson, R. D. Cook, C. S. Dutcher, A. P. Ault, *Anal. Chem.* **2018**, *90*, 11232 – 11239.
[72] R. M. Garland, M. E. Wise, M. R. Beaver, H. L. DeWitt, A. C. Aiken, J. L. Jimenez, M. A. Tolbert, *Atmos. Chem. Phys.* **2005**, 11.
[73] V. F. McNeill, R. L. N. Yatavelli, J. A. Thornton, C. B. Stipe, O. Landgrebe, *Atmos. Chem. Phys.* **2008**, *8*, 5465 – 5476.
[74] Y. Qiu, N. Odendahl, A. Hudait, R. Mason, A. K. Bertram, F. Paesani, P. J. DeMott, V. Molinero, *J. Am. Chem. Soc.* **2017**, *139*, 3052 – 3064.

Manuscript received: July 1, 2021
Accepted manuscript online: August 16, 2021
Version of record online: October 4, 2021

